Theor Chem Acc (2011) 130:83–93
DOI 10.1007/s00214-011-0973-1

REGULAR ARTICLE

Assessing group-based cutoffs and the Ewald method for electrostatic interactions in clusters and in saturated, superheated, and supersaturated vapor phases of dipolar molecules

Mohammadhasan Dinpajooh · Samuel J. Keasler · Donald G. Truhlar · J. Ilja Siepmann

Received: 12 March 2011 / Accepted: 2 June 2011 / Published online: 8 July 2011

Abstract Monte Carlo simulations in the canonical, isobaric-isothermal, grand canonical, and Gibbs ensembles were used to assess whether the computationally expensive Ewald summation method for the computation of the first-order electrostatic energy can be replaced with a simpler truncation approach for accurate simulations of the saturated, superheated, and supersaturated vapor phases of dipolar and hydrogen-bonding molecules. Rotationally averaged hydrogen fluoride dimer and trimer energies, thermophysical properties and aggregation in the superheated vapor phase of hydrogen fluoride, nucleation free energy barriers for water, and the vapor–liquid coexistence properties of hydrogen fluoride and water were investigated over a wide range of state points. We find that for densities not too close to the critical density, results obtained from simulations using a spherical potential truncation based on neutral groups (molecules or fragments) for the Coulomb interactions are statistically identical to those obtained using the Ewald summation method. Use of the simpler spherical truncation results in a significant reduction of the computational effort for simulations employing molecular mechanics force fields and also allows for straightforward implementation of many-body expansion methods to compute the potential energy from electronic structure calculations of subsystems of the entire vapor-phase system.

Keywords Molecular simulations · Electrostatic energy · Dipolar molecules · Ewald summation

M. Dinpajooh · S. J. Keasler · D. G. Truhlar · J. I. Siepmann (✉)
Department of Chemistry and Chemical Theory Center, University of Minnesota, 207 Pleasant St SE, Minneapolis, MN 55455-0431, USA
e-mail: siepmann@umn.edu

M. Dinpajooh
e-mail: dinpa001@umn.edu

S. J. Keasler
e-mail: keasl002@umn.edu

D. G. Truhlar
e-mail: truhlar@umn.edu

J. I. Siepmann
Department of Chemical Engineering and Materials Science, Chemical Theory Center, University of Minnesota, 207 Pleasant St SE, Minneapolis, MN 55455-0431, USA

1 Introduction

In molecular simulations of bulk phases, it is customary to divide the interactions into short-range and long-range parts where the short-range interactions are usually truncated at a distance that is smaller than half of the linear dimension of the periodically replicated simulation cell [1, 2]. Such calculations commonly employ the minimum image convention. In many molecular mechanics force fields, the intermolecular interactions include terms for the short-range exchange repulsion and the medium-range dispersion-like attraction; taken together, these two kinds of terms are often called van der Waals (vdW) interactions (e.g., a Lennard-Jones potential). The other terms in the potential represent the long-range electrostatic interactions of permanent multipoles.

For vdW interactions, the repulsive and attractive parts are explicitly evaluated up to the potential truncation distance, and the contributions beyond this cutoff distance are commonly approximated by analytical tail corrections that assume that the pair distribution functions have converged

to unity for distances beyond the potential truncation [1, 2]. Since the distance used for the potential truncation of the vdW interactions should be much larger than the minimum-energy separation for the underlying pairwise potential function, the interactions beyond the truncation distance are always attractive and lower the potential energy, and the contribution from the tail correction to the system's internal energy and pressure can be significant.

Electrostatic interactions may be divided into first-order effects, which are "static" interactions between permanent multipole moments, and higher-order effects, representing induction, also called "polarization". Here, we do not include polarization explicitly, although it could be included implicitly in the parameterized treatment of vdW interactions. For the first-order electrostatic interactions (sometimes called Coulomb energy in the discussion below), the situation is more complex than that for vdW interactions. Although the electrostatic interactions (up to the quadrupole–quadrupole term) decay more slowly with distance than the dispersion-like interactions, they can make a positive or negative contribution to the internal energy and pressure depending on the sign for charged particles and the orientation for dipoles and higher multipoles. The Ewald summation (ES) technique is the method of choice for the accurate evaluation of the first-order electrostatic interactions of charged or dipolar particles in condensed phases [1–5]. In the ES technique, the conditionally convergent sums over Coulomb interactions are split into a real-space part involving only pairs within a spherical truncation distance (or just using the minimum image convention) and a Fourier part involving a sum over reciprocal lattice vectors. The main drawback of the ES technique is a significant increase in the computational cost compared to simple truncation methods. Special techniques have been developed to reduce the dependence of such lattice summation techniques on the system size [6, 7].

Many studies have investigated how one may reduce the cost increase associated with the ES technique, but results have been mixed for condensed phase systems [8–14]. In the present article, we address the question of whether less expensive techniques can be used to accurately treat first-order electrostatic interactions for a vapor phase containing dipolar and hydrogen-bonding molecules. Our motivation is to reduce the cost for simulation studies of vapor-phase aggregation [15, 16] (e.g., for hydrogen fluoride and acetic acid), of vapor-to-particle nucleation processes [17, 18], and of vapor–liquid phase equilibria using the Gibbs ensemble [19–21]. In particular, we would like to enable the use of electronic structure methods to describe the interactions in these vapor-phase systems where treating the large and mostly empty space becomes very expensive for plane-wave-based simulations [22–24].

The simpler method we test here is the use of a neutral-group-based (NGB) cutoff. In this method, we define a set of electrically neutral groups (monomers), and each such group is assigned a principal interaction site. Then all Coulomb interactions between group A and group B are neglected if their principal interactions sites are separated by more than a cutoff distance, r_{cut}. (This is essentially the same as what is called a residue-based cutoff [25] in some biomolecular simulation programs, except that residues are restricted to integer charges, and NGB groups are restricted to zero charge.)

The electrostatically embedded many-body (EE–MB) method [26–29] is a promising alternative to extended plane wave calculations. In EE-MB, the total electronic energy of the system is calculated by computing explicitly the electronic energies for small groups (dimers or trimers) of molecules or molecular fragments (monomers) in an electric field representing the other fragments not explicitly included in a given oligomer. The implementation of the EE–MB method for periodic systems would benefit from the use of a truncation scheme for the inclusion of fragments in the embedding field. Furthermore, a better understanding of the effects of truncation schemes for dipolar interactions may enable a more efficient implementation of the EE-MB approach by reducing the number of dimer or trimer calculations (i.e., the many-body calculations would only be carried out when the monomers are within a specific truncation sphere).

In this study, we investigate the distance dependence of the rotationally averaged energy for hydrogen fluoride dimers and trimers, the thermophysical properties in the superheated vapor phase of hydrogen fluoride, the vapor-to-liquid nucleation free energy barrier for water, and the vapor–liquid equilibria for hydrogen fluoride and for water. The remainder of the paper is organized as follows: In the next section, the simulation details are summarized. In Sect. 3, the results of simulations are discussed, and Sect. 4 summarizes the main conclusions.

2 Simulation details

The MCCCS–MN (Monte Carlo for Complex Chemical Systems–Minnesota) software program [30] developed by the Siepmann group was used for all simulations. Hydrogen fluoride and water are represented by the OPLS (optimized potentials for liquid simulations) [31] and TIP4P (transferable intermolecular potentials—four point) [32] models, respectively, developed by Jorgensen and coworkers. Both models use a rigid internal structure and a single Lennard-Jones 12–6 interaction site per molecule at the fluorine or the oxygen position. The first-order electrostatic interactions are represented for both models by

three partial charges; for hydrogen fluoride, these are placed on the atomic centers with an additional site on the bond vector close to the fluorine atom; and for water, the partial charges are placed on the positions of the two hydrogen atoms and an additional site on the bisector of the HOH angle close to the oxygen atom.

We consider four cases below. The first case (Sect. 2.1) is a reduced dimensional model system treated in the canonical ensemble. The next three cases are treated in the isobaric–isothermal, grand canonical, and Gibbs ensembles, and in these cases, the ES technique is considered as the standard against which truncation schemes are compared. The convergence (and efficiency) of the ES technique implemented in the MCCCS–MN program is controlled by three parameters: (i) the real-space cutoff, r_{cut}, that can be adjusted to shift the burden of the computation between real-space and reciprocal-space parts, (ii) the Ewald convergence parameter, κ, that controls the width of the continuous Gaussian charge distributions used to compensate for the (partial) point charges, and (iii) the number of reciprocal lattice vectors, k_{max}, that is set to $\lceil \kappa L_{box} \rceil$ (where $\lceil\rceil$ and L_{box} are the ceiling function giving the smallest integer number not less than the argument and the length of the (cubic) simulation box, respectively). Note that κ is set to $3.2/r_{cut}$ here, a value that yields appropriate convergence for typical systems [1]. Therefore, a smaller value of r_{cut} results in larger values of κ and k_{max} (i.e., a broader Gaussian width for the real-space calculations and more reciprocal lattice vectors). For the simulations in the isobaric–isothermal ensemble, the value of k_{max} fluctuates in conjunction with L_{box}. The ES real-space cutoff is applied individually to every site–site pair (in contrast to the NGB cutoff procedure).

It should be noted here that special versions of the conventional Ewald summation remain the method of choice for Monte Carlo simulations, whereas the smooth particle mesh Ewald method [7] has now become the standard for molecular dynamics simulations of large systems. The reason is that Monte Carlo simulations require the efficient calculation of the energy difference for small parts of the entire system, e.g., a translational or rational move acts only on a single molecule and many biased Monte Carlo moves involve decision-making based on the energy for a single interaction site, whereas the total energy of the entire system is only computed for volume moves. The conventional Ewald method can be readily adapted so that the cost of the energy calculation scales with the relative size of the fragment involved in the specific Monte Carlo move.

For the Lennard-Jones interactions, a site–site based truncation and tail corrections for the energy and pressure evaluations are used. Since Monte Carlo simulations do not require continuous energy functions, there is no need for a switching function to smoothly truncate the energy at the cutoff, i.e., both the Coulomb and Lennard-Jones interactions are calculated and fully included for separations up to r_{cut} and not calculated (set to zero) for separations beyond. The MCCCS–MN program uses the same value of r_{cut} for the truncation of the Coulomb interactions (either using the ES technique or the NGB approach) and the Lennard-Jones interactions.

2.1 Dimers and trimers of hydrogen fluoride

Metropolis Monte Carlo simulations [33] for either two or three hydrogen fluoride molecules were performed at constant temperature; 260, 520, and 1040 K were used for the two-molecule system and only 260 K for the three-molecule system. In these simulations, the center-of-mass separations of the molecules are fixed, and only rotational moves of individual molecules (using the COM as the origin for the rotation) were used. For each combination of temperature and COM separation, the dimer and trimer simulations consisted of 10^7 and 1.2×10^8 Monte Carlo trial moves, respectively. For these cluster simulations, all pair interactions were explicitly evaluated and no potential truncation was applied.

2.2 Superheated vapor phase of hydrogen fluoride and liquid phases of hydrogen fluoride and water

Monte Carlo simulations in the isobaric–isothermal ensemble [34] were carried out for a system consisting of 108 hydrogen fluoride molecules at $P = 15.5$ kPa and $T = 240$, 260, and 280 K. At these state points, hydrogen fluoride is in what is often called a superheated vapor phase, i.e., the temperature is above the boiling point for the specific pressure. At conditions above but close to the boiling point, aggregation is known to be prevalent in the vapor phase of hydrogen fluoride [35]. Such aggregation behavior can cause sampling problems, and the aggregation-volume-bias Monte Carlo (AVBMC) approach [36, 37] in combination with the configurational-bias Monte Carlo (CBMC) scheme [38, 39] was used to improve the sampling of phase space for hydrogen fluoride under these conditions. The simulations included volume, AVBMC, translational, and rotational moves with the move type being selected at random with probabilities of 0.0018, 0.4982, 0.25, and 0.25, respectively. Each simulation consisted of 10^5 and 5×10^6 MC cycles for the equilibration and production periods, respectively (each cycle consists of N trial moves, where N is the number of molecules in the system). Five independent simulations were carried out for each combination of state point and method for the computation of the electrostatic interactions. In order to investigate the effect of the spherical truncation

distance for the NGB cutoff on the simulations when ES was not used, cutoff distances ranging from 4 to 48 Å were considered, where the truncation for Coulomb interactions was applied based on the F–F distance. For the production simulations with the ES method, r_{cut} was set to approximately 0.3 L_{box}. To assess the influence of r_{cut} on the efficiency of the ES method, additional shorter simulations were carried out with $r_{cut} \approx 0.4\ L_{box}$ and $r_{cut} = 14$ Å (this is the standard value used for condensed phase simulations with the TraPPE force field [40]).

For comparison, isobaric–isothermal ensemble Monte Carlo simulations were also carried out for the liquid phase of hydrogen fluoride at $T = 260$ K and $P = 101.3$ kPa and water at $T = 300$ K and $P = 101.3$ kPa. To enable the investigation of spherical truncation distances of up to 16 Å, a larger system size of 1,500 molecules was used for these liquid-phase simulations. Volume, translational, and rotational moves [34] were employed for these simulations with the probability for selecting a volume move being set to 0.00014 and the remainder equally divided between the other two move types. AVBMC moves are not needed for the liquid phase because this phase does not possess the spatial microheterogeneity characteristic of the superheated phase that contains monomers and aggregates separated by large amounts of empty space. Again, five independent simulations were carried out for every truncation scheme, and each consisted of 10^5 MC cycles for the equilibration and production periods. For simulations with the NGB truncation, F–F distance cutoffs ranging from 4 to 16 Å were evaluated. For simulations with the ES method, real-space cutoffs at 8, 12, and 14 Å were explored.

2.3 Vapor-to-liquid nucleation free energies for water

Simulations in the grand canonical ensemble using the aggregation-volume-bias Monte Carlo algorithm with self-adaptive umbrella sampling and histogram reweighting (AVUS-HR) [41] were performed for the TIP4P water model at 260 K to examine the effect of the NGB cutoff on vapor-to-liquid nucleation free energies. The simulations consisted of 8×10^6 Monte Carlo trial moves divided evenly between AVBMC/CBMC insertions, AVBMC/CBMC deletions, translations, and rotations. The upper bound on the number of molecules in the grand canonical simulations was set to 100, and a Stillinger-type [42], energy-based cluster criterion for pairs of molecules at $-260\ k_B$ K (equivalent to a pair energy of -2.16 kJ/mol) was enforced as a measure of aggregation. It should be noted here that the AVUS-HR simulations use an adapted form of the grand canonical ensemble formalism where the volume of the simulation box does not need to be specified because the simulation box contains a single cluster (surrounded by vaccuum) that is defined by the Stillinger criterion (and, hence, does not involve the use of a periodically replicated system) [41]. Particularly for strongly aggregating systems, the choice of cluster criterion has only a minor impact on the simulation results [41, 43]. Simulations were carried out for five different values of the NGB truncation distance: $r_{cut} = 6$, 8, 10, 12, and ∞ Å (the last corresponds to explicitly including all pair energies irrespective of separation distance—a choice that is possible in the AVUS-HR simulations of a single cluster). The NGB truncation for the Coulomb interactions is based on the M–M distance (where M is the site carrying the negative partial charge).

2.4 Vapor–liquid phase equilibria for water and hydrogen fluoride

Gibbs ensemble Monte Carlo (GEMC) simulations, which utilize two separate periodic simulation boxes in thermodynamic contact without an explicit interface [19, 20], were carried out in order to compute the vapor–liquid coexistence densities, saturated vapor pressures, and heats of vaporization for hydrogen fluoride and water. In addition to volume exchange, translational and rotational moves, these simulations employed CBMC particle swaps [44, 45] between the boxes and, only for hydrogen fluoride, AVBMC/CBMC moves in the vapor phase. The systems contained 1000 molecules and four independent simulations were carried out at each state point for which 5×10^4 MC cycles were used for the equilibration periods for both compounds, and 5×10^4 and 2.4×10^5 MC cycles were used for the production periods of the water and hydrogen fluoride systems, respectively. The ES technique with $r_{cut} = 14$ Å was used for the computation of the Coulomb interactions in the liquid phase for all simulations, whereas we explored use of the ES technique and of NGB cutoffs ($r_{cut} = 14$ Å based on the M–M distance for water and 24 Å based on the F–F distance for hydrogen fluoride) for the vapor-phase box that contained on average between 30 and 300 molecules.

3 Results and discussion

For any fixed relative orientation, the interaction energy of two dipoles decays as r^{-3}. The orientational average of the interaction energy for random relative orientations of the two point dipoles is zero; however, for two interacting molecules, the distribution is not random at finite temperature, and Boltzmann averaging of the orientations leads to a dipole–dipole interaction energy that decays as r^{-6} when the thermal energy exceeds the magnitude of the potential energy of interaction [46] (this is sometimes called the Keesom potential). However, the influence of neighboring

molecules and cooperative effects each make the orientationally averaged term more long-ranged [47, 48]. In the liquid phase, each molecule influences the orientational distribution of its neighbors, the neighbors influence the orientation of their neighbors, and so forth. Thus, the orientational correlation becomes long ranged in the liquid phase, and methods such as ES are necessary to treat dipole–dipole interactions. In the present study, the focus is on treating electrostatic interactions of dipolar molecules in the vapor phase.

3.1 Dimers and trimers of hydrogen fluoride

In order to generate information about the magnitude of the Boltzmann-averaged dipole–dipole interaction energy and to make decissions about a suitable truncation distance, we have investigated dimers and trimers of hydrogen fluoride with fixed center-of-mass separation. It should be noted that, as is typical of most dipolar molecules, the center of mass does not coincide with the center of charge for the specific models used here.

Figure 1 shows a log–log plot of the Boltzmann-averaged Coulomb energy of the hydrogen fluoride dimer as a function of separation at three different temperatures. For separations larger than about 6 Å, the log–log plots are linear with a slope of −6, i.e., the Boltzmann-averaged Coulomb energy decays as r^{-6}, as expected for the Keesom potential. At shorter separations, the graphs exhibit some curvature, and the magnitude of the slopes decreases with decreasing separation (see inset of Fig. 1). This signals that the Coulomb energies for favorable orientations are becoming comparable in magnitude to the thermal energy and that the orientational distribution is becoming less uniform. This is most evident for the lowest temperature investigated here, but even at $T = 260$ K, the instantaneous slope in the region of 2.5 Å $< r <$ 4 Å appears to be closer to −4 than the value of −3 corresponding to a fixed relative orientation of two point dipoles. At $T = 260$ K, the magnitude of the Boltzmann-averaged Coulomb energy falls below 10 K (in thermal units) for $r > 8$ Å, below 2.6 K for $r > 10$ Å, below 1 K for $r > 12$ Å, and below 0.1 K for $r > 17$ Å, but Coulomb energies for specific orientations can be much larger (e.g., the Coulomb energy for the most favorable orientation at $r = 8$ Å is −117 K). Nevertheless, the small values for the Boltzmann averages indicate that a NGB truncation at distances larger than, say, 10 Å should have negligible influence (i.e., an error of less than $0.01 k_B T$ for the averaged interaction energy) on thermodynamic averages for the vapor phases of small dipolar molecules and, hence, may also be used to reduce the number of dimer or trimer calculations and the number of fragments contributing to the embedding field in the EE-MB approach. For larger molecules where the dipole moment may results from a charge distribution that is spread over larger intramolecular distances, a correspondingly larger cutoff distance should be used for the NGB truncation.

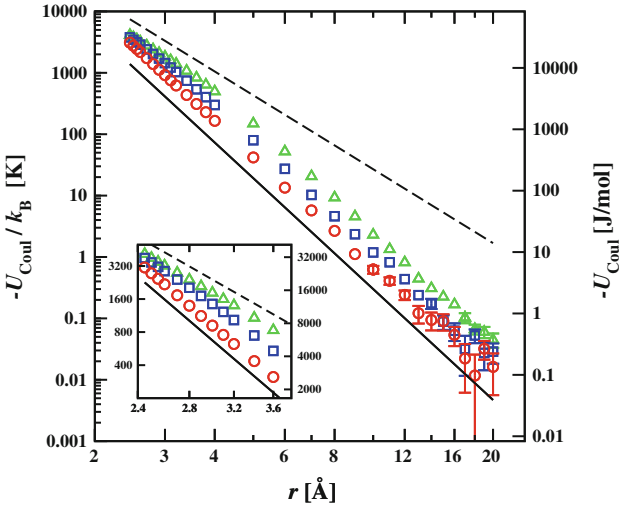

Fig. 1 Boltzmann-averaged Coulomb energy for the hydrogen fluoride dimer versus center-of-mass separation. Data at $T = 260$, 540, and 1040 K are indicated by *green triangles*, *blue squares*, and *red circles*, respectively. *Error bars* correspond to the standard error of the mean and are only shown when larger than the symbol size. The *solid* and *dashed lines* indicate slopes of −6 and −4, respectively. The *inset* magnifies the data at short range

Table 1 Boltzmann-averaged Coulomb energy for a pair of hydrogen fluoride molecules at separation r_{12} (rows) interacting with a third molecule at separation $r_{13} = r_{23}$ (columns)

$r_{12}\backslash r_{13}$	6	9	12	16	∞
3	−15,177 ± 4	−15,176 ± 4	−15,173 ± 2	−15,172 ± 4	−15,174 ± 6
4	−4,058 ± 2	−4,132 ± 2	−4,135 ± 2	−4,136 ± 2	−4,131 ± 2
5	−1,167 ± 1	−1,234 ± 1	−1,240 ± 1	−1,240 ± 1	−1,237 ± 1
6		−428.6 ± 0.4	−431.8 ± 0.4	−432.6 ± 0.4	−431.6 ± 0.3
8		−75.4 ± 0.2	−77.1 ± 0.2	−77.4 ± 0.2	−77.4 ± 0.2
10			−19.9 ± 0.1	−20.0 ± 0.1	−20.1 ± 0.1

Energies and distances are given in units of J/mol (per mole of dimers) and Å, respectively. The temperature is 260 K

As an additional test, we have investigated systems consisting of three interacting hydrogen fluoride molecules with their fixed center-of-mass positions arranged to form an isosceles triangle that satisfies $r_{12} < r_{13} = r_{23}$. We computed the Boltzmann-averaged Coulomb energy for the pair of molecules 1 and 2 as a function of separation at $T = 260$ K for four different values of r_{13}, in particular, 6, 9, 12, and 16 Å, and we compare to the dimer data. As can be seen from the numerical data summarized in Table 1, the influence of the third molecule on the properties of the "dimer" is negligible for $r_{13} \geq 12$ Å, but the simulations for $r_{13} = 6$ Å and $r_{12} = 4$ or 5 Å yield pair energies that are significantly smaller in magnitude (and the same holds true for $r_{13} = 9$ Å and $r_{12} = 5$, 6, or 8 Å), i.e., a truncation error is encountered when r_{12} approaches the value of r_{13}. For $r_{13} \geq 12$ Å, we do not find any significant differences between the orientational distributions of the "dimer" in the three-molecule system and in the two-molecule system (data not shown). The negligible differences observed in the presence of a somewhat distant third molecule further support the conclusion that NGB truncation may be used to reduce the number of calculations for the EE-MB approach.

3.2 Superheated vapor of hydrogen fluoride and liquid phases of hydrogen fluoride and water

Hydrogen fluoride can form strong hydrogen bonds [49, 50], and due to the formation of hydrogen-bonded aggregates, it belongs to the class of strongly associating fluids that show large deviations from ideal gas behavior near the saturation line [24, 51]. Evidence of extensive association in the vapor phase of hydrogen fluoride has been known for nearly ninety years [35]. This makes the superheated vapor phase of hydrogen fluoride a particularly appropriate choice for this study.

Some of the thermodynamic data obtained from the simulations with different cutoff distances for the NGB truncation and with the ES technique are listed in Table 2. For the three temperatures investigated here, the data indicate that $r_{cut} \geq 6$ Å is sufficient to yield thermodynamic averages that coincide with those obtained for the ES technique. In contrast, the simulations with $r_{cut} = 4$ Å consistently yield average energies that are smaller and molar volumes that are larger than those for simulations that are converged with respect to the treatment of the electrostatic interactions, but these deviations decrease with increasing temperature. The simulations with $r_{cut} = 5$ Å deviate from the ES results mostly in the opposite direction than those with $r_{cut} = 4$ Å, but the deviation is much smaller, and agreement with the ES simulations is satisfactory for the two higher temperatures.

Table 2 Thermodynamic properties of the superheated vapor phase of hydrogen fluoride ($P = 15.5$ kPa): ensemble averages of the Coulomb and Lennard Jones energies, and the molar volume with their standard errors of the mean

r_{cut} (Å)	T (K)	U_{Coul} (kJ/mol)	U_{LJ} (kJ/mol)	$V_m/100$ (cm^3/mol)
4	240	−23.86 ± 0.07	5.17 ± 0.02	490 ± 1
5		−25.44 ± 0.07	5.10 ± 0.01	411 ± 4
6		−25.10 ± 0.06	5.08 ± 0.02	435 ± 2
8		−25.18 ± 0.05	5.08 ± 0.01	430 ± 2
16		−25.21 ± 0.08	5.10 ± 0.02	431 ± 4
24		−25.21 ± 0.04	5.08 ± 0.01	432 ± 2
36		−25.19 ± 0.10	5.08 ± 0.03	431 ± 4
48		−25.12 ± 0.10	5.07 ± 0.02	433 ± 4
ES		−25.12 ± 0.08	5.07 ± 0.02	433 ± 3
4	260	−9.35 ± 0.07	2.02 ± 0.02	1,027 ± 1
5		−11.57 ± 0.07	2.36 ± 0.01	941 ± 2
6		−11.38 ± 0.10	2.31 ± 0.03	947 ± 4
8		−11.50 ± 0.10	2.33 ± 0.03	944 ± 3
16		−11.59 ± 0.08	2.35 ± 0.02	941 ± 3
24		−11.45 ± 0.15	2.32 ± 0.04	944 ± 6
36		−11.38 ± 0.14	2.31 ± 0.03	948 ± 6
48		−11.56 ± 0.13	2.34 ± 0.03	944 ± 4
ES		−11.51 ± 0.04	2.33 ± 0.01	941 ± 3
4	280	−1.62 ± 0.05	0.33 ± 0.01	1,418 ± 1
5		−1.85 ± 0.07	0.37 ± 0.02	1,405 ± 2
6		−1.80 ± 0.04	0.36 ± 0.01	1,410 ± 2
8		−1.89 ± 0.07	0.37 ± 0.02	1,405 ± 3
16		−1.76 ± 0.06	0.35 ± 0.01	1,408 ± 4
24		−1.92 ± 0.10	0.38 ± 0.03	1,404 ± 4
36		−1.82 ± 0.07	0.36 ± 0.02	1,407 ± 2
48		−1.83 ± 0.08	0.36 ± 0.02	1,404 ± 1
ES		−1.96 ± 0.07	0.39 ± 0.02	1,408 ± 2

The simulations in Table 2 yield cohesive energies of 20.1, 9.2, and 1.6 kJ/mol at 240, 260, and 280 K, respectively, indicating that aggregation has led to the formation of about one, one half, and one tenth, respectively, of a hydrogen bond per molecule in these phases. The compressibility factors ($Z = pV_m/RT$, where R and V_m are the ideal gas constant and the molar volume, respectively) are found to be 0.336, 0.675, and 0.937, respectively. Compressibility factors smaller than unity indicate that attractive interactions have resulted in aggregation (and, hence, deviations from the ideal gas law). Given the indication of strong aggregation (Z is far from unity at the two lower temperatures), it is important to verify that the correct aggregate size distributions can be obtained with the spherical truncation schemes. To this extent, a hydrogen bond was considered to be present when the H–F distance

between two molecules is smaller than 2.3 Å, which is the position of the first minimum in the intermolecular part of the H–F radial distribution function. Although aggregate size distributions for this and similar systems are known to depend somewhat on the precise criterion used to identify a hydrogen bond [24, 52], here we are solely interested in comparing different truncation schemes, and the use of the simple H–F distance criterion is therefore adequate. Aggregate size distributions are reported as the fraction of aggregates of a given size, i.e., the ratio of the number of aggregates of a given size to the total number of aggregates. The fraction of clusters of a given size can be used to compute directly the pseudo-equilibrium constants that are input parameters for equations of state that describe the vapor of associating fluids in terms of an equilibrium mixtures of clusters [53].

The computed fractions of monomers and aggregates (from dimers to hexamers) are reported in Table 3. In agreement with the trend for the compressibility factors, the fraction of monomers increases and the average cluster size decreases with increasing temperature. At $T = 240$ K, about one quarter of the aggregates are tetramers and an appreciable fraction of even larger aggregates is present. In contrast, the size distribution decays monotonically at $T = 280$ K. The data for $r_{cut} \geq 6$ Å agree satisfactorily with those obtained for the ES technique (at $T = 260$ K, the fractions of hexamers for $r_{cut} = 6$ Å and the ES method fall just outside of their combined uncertainty estimates; at $T = 280$ K, the fraction of hexamers is extremely low and the relative uncertainties are large, but the fraction of hexamers for $r_{cut} = 6$ Å agrees very well with the value obtained by averaging over the x_6 values for the three largest cutoffs and the ES method). The aggregate size distributions also explain the large deviations observed in the thermodynamic properties for $r_{cut} = 4$ Å, i.e., this extremely small cutoff leads to a dramatic decrease in the population of pentameric and larger aggregates because the linear extension of these aggregates (even when they are cyclic) exceeds the truncation distance and, hence, some of the favorable dipole–dipole interactions in these larger clusters would not be included.

Now that we have confirmed that the use of a NGB truncation with $r_{cut} \geq 6$ Å yields accurate thermodynamic and structural properties for the superheated vapor phase of hydrogen fluoride, we can address the gain in efficiency. For the 108-molecule simulations at $T = 240$ and 280 K, the (fluctuating) box lengths are close to 200 and 300 Å, respectively. Using the ES technique with $r_{cut} \approx 0.4\ L_{box}$ results in an average of about 1200 reciprocal lattice vectors and a CPU time requirement that is about five times larger than that for the corresponding simulation with the NGB truncation scheme and $r_{cut} = 8$ Å. Using a larger

Table 3 Aggregate size distribution for the superheated vapor phase of hydrogen fluoride vapor ($P = 15.5$ kPa): percentages of monomeric to hexameric clusters with their standard errors of the mean

r_{cut} (Å)	T (K)	x_1 (%)	x_2 (%)	x_3 (%)	x_4 (%)	x_5 (%)	x_6 (%)
4	240	49.0 ± 0.2	3.33 ± 0.04	7.2 ± 0.2	30.9 ± 0.5	6.0 ± 0.1	1.7 ± 0.1
5		43.7 ± 0.2	2.69 ± 0.03	5.3 ± 0.1	24.9 ± 0.5	15.3 ± 0.2	4.2 ± 0.2
6		44.2 ± 0.4	2.74 ± 0.06	5.6 ± 0.1	25.5 ± 0.6	14.9 ± 0.5	5.2 ± 0.4
8		44.1 ± 0.2	2.70 ± 0.04	5.6 ± 0.2	24.4 ± 0.5	14.3 ± 0.3	5.4 ± 0.4
24		44.0 ± 0.2	2.69 ± 0.02	5.5 ± 0.1	24.6 ± 0.5	14.7 ± 0.4	5.3 ± 0.3
48		44.2 ± 0.3	2.72 ± 0.05	5.6 ± 0.2	25.9 ± 0.8	13.7 ± 0.6	4.8 ± 0.3
ES		44.2 ± 0.3	2.74 ± 0.04	5.5 ± 0.2	25.8 ± 0.4	13.5 ± 0.7	5.1 ± 0.4
4	260	85.0 ± 0.1	4.24 ± 0.02	3.80 ± 0.06	5.8 ± 0.2	0.8 ± 0.1	0.16 ± 0.03
5		82.3 ± 0.1	3.99 ± 0.02	3.56 ± 0.02	6.9 ± 0.1	2.7 ± 0.1	0.48 ± 0.03
6		82.6 ± 0.2	4.00 ± 0.03	3.62 ± 0.03	6.9 ± 0.2	2.4 ± 0.1	0.52 ± 0.04
8		82.3 ± 0.2	4.01 ± 0.03	3.57 ± 0.05	6.9 ± 0.2	2.5 ± 0.1	0.57 ± 0.04
24		82.4 ± 0.2	4.02 ± 0.02	3.60 ± 0.02	6.8 ± 0.2	2.3 ± 0.1	0.63 ± 0.06
48		82.3 ± 0.2	3.99 ± 0.04	3.59 ± 0.04	6.8 ± 0.1	2.5 ± 0.2	0.58 ± 0.04
ES		82.3 ± 0.1	4.02 ± 0.02	3.61 ± 0.03	6.9 ± 0.2	2.3 ± 0.1	0.60 ± 0.03
4	280	96.18 ± 0.06	2.63 ± 0.02	0.75 ± 0.01	0.40 ± 0.04	0.03 ± 0.01	0.003 ± 0.001
5		95.95 ± 0.07	2.62 ± 0.01	0.84 ± 0.04	0.50 ± 0.05	0.08 ± 0.02	0.009 ± 0.002
6		96.00 ± 0.05	2.62 ± 0.01	0.82 ± 0.02	0.47 ± 0.04	0.07 ± 0.01	0.013 ± 0.002
8		95.93 ± 0.07	2.60 ± 0.01	0.85 ± 0.04	0.52 ± 0.03	0.09 ± 0.02	0.008 ± 0.003
24		95.90 ± 0.09	2.60 ± 0.01	0.83 ± 0.04	0.59 ± 0.08	0.08 ± 0.02	0.011 ± 0.005
48		95.95 ± 0.06	2.62 ± 0.01	0.85 ± 0.03	0.50 ± 0.06	0.07 ± 0.03	0.008 ± 0.006
ES		95.89 ± 0.06	2.60 ± 0.01	0.81 ± 0.03	0.52 ± 0.05	0.14 ± 0.03	0.024 ± 0.012

Table 4 Thermodynamic properties of the liquid phase of hydrogen fluoride at 260 K and 101.3 kPa and of water at 300 K and 101.3 kPa: ensemble averages of the Coulomb and Lennard Jones energies, and the molar volume with their standard errors of the mean

Compound	Method	r_{cut} (Å)	U_{Coul} (kJ/mol)	U_{LJ} (kJ/mol)	V_m (cm^3/mol)
HF	NGB	4	−34.69 ± 0.03	1.880 ± 0.006	14.85 ± 0.03
	NGB	5	−34.44 ± 0.04	2.461 ± 0.002	16.03 ± 0.04
	NGB	6	−31.60 ± 0.02	2.461 ± 0.003	17.20 ± 0.03
	NGB	8	−30.48 ± 0.01	2.524 ± 0.006	18.12 ± 0.03
	NGB	16	−29.82 ± 0.01	2.596 ± 0.005	18.78 ± 0.03
	ES	8	−29.66 ± 0.01	2.600 ± 0.005	18.83 ± 0.02
	ES	12	−29.66 ± 0.01	2.600 ± 0.005	18.83 ± 0.03
	ES	14	−29.66 ± 0.01	2.605 ± 0.004	18.85 ± 0.03
H_2O	NGB	4	−58.51 ± 0.04	7.609 ± 0.020	14.15 ± 0.02
	NGB	5	−54.68 ± 0.05	7.957 ± 0.019	16.61 ± 0.02
	NGB	6	−51.28 ± 0.02	7.589 ± 0.005	17.57 ± 0.02
	NGB	8	−49.80 ± 0.02	7.409 ± 0.008	17.89 ± 0.02
	NGB	16	−48.76 ± 0.02	7.216 ± 0.005	18.42 ± 0.01
	ES	8	−48.57 ± 0.02	7.295 ± 0.008	18.15 ± 0.01
	ES	12	−48.56 ± 0.02	7.299 ± 0.006	18.17 ± 0.01
	ES	14	−48.57 ± 0.01	7.291 ± 0.003	18.14 ± 0.01

value of r_{cut} for the latter scheme has only a relatively modest effect (e.g., an increase in the CPU requirement of about 10 % when changing to $r_{cut} = 48$ Å because the MCCCS–MN program uses a hierarchy of cutoffs to avoid unnecessary distance calculations [54]). In contrast, using a smaller value of r_{cut} for the simulations with the ES technique can result in a dramatic increase of the CPU time requirement. For example, with $r_{cut} = 14$ Å, the average number of reciprocal vectors increases to about 2×10^5 and 6×10^7 for the simulations at 240 and 280 K, respectively, and CPU time increases by factors of about 50 and 170 compared to the simulations with the NGB truncation scheme and $r_{cut} = 8$ Å.

To illustrate that the NGB truncation method should not be used for condensed phase simulations, thermodynamic data for the liquid phases of hydrogen fluoride and water are presented in Table 4. Cooperative effects in the liquid phase result in a slower decay of the orientational correlation with distance [47, 48]. Thus, the simulations with a NGB cutoff at 6 Å yield very large deviations from the data obtained with the ES method. The deviations slowly decrease with increasing NGB cutoff but even the simulations with $r_{cut} = 16$ Å, the largest value that is safely less than half of the fluctuating box length (about 36 Å for both systems), still exhibit rather significant deviations. In contrast, the simulations employing the ES technique with different real-space cutoff values show excellent agreement.

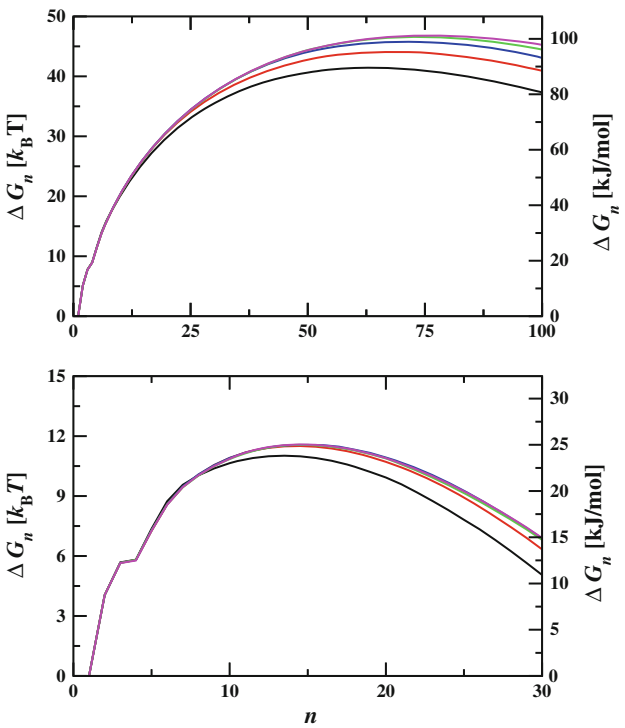

Fig. 2 Nucleation free energy profiles for the TIP4P water model at $T = 260$ K and a grand canonical reservoir density of 3.5×10^{-7} molecules/Å^3 (*top panel*) or 1.0×10^{-6} molecules/Å^3 (*bottom panel*) are shown for cutoffs of 6, 8, 10, 12, and ∞ Å in *black*, *red*, *blue*, *green*, and *magenta*, respectively

3.3 Vapor-to-liquid nucleation free energies for water

Figure 2 shows the nucleation free energy profiles as function of the cluster size, n, for water computed using the AVUS-HR method at two vapor densities (i.e., supersaturation ratios). The nucleation free energy, ΔG_i is defined as the free energy change to form a cluster containing i molecules from a vapor phase of monomers at a defined chemical potential and can be obtained from the cluster size distribution using [55, 56]

Table 5 Nucleation free energy barriers and critical cluster sizes with their standard errors of the mean for water at $T = 260$ K for reservoir densities of 3.5×10^{-7} and 1.0×10^{-6} molecules/Å^3

ρ_{gas} (molecules/Å^3)	r_{cut} (Å)	ΔG^* (k_BT)	ΔG^* (kJ/mol)	n^* (molecules)
3.5×10^{-7}	6	41.4 ± 0.4	89.5 ± 0.8	64 ± 1
	8	44.1 ± 0.2	95.3 ± 0.4	68 ± 1
	10	45.8 ± 0.1	98.9 ± 0.3	71 ± 2
	12	46.6 ± 0.1	100.8 ± 0.2	74 ± 2
	∞	46.8 ± 0.2	101.2 ± 0.3	76 ± 2
1.0×10^{-6}	6	11.02 ± 0.07	23.8 ± 0.2	13.5 ± 0.2
	8	11.52 ± 0.04	24.9 ± 0.1	14.3 ± 0.2
	10	11.59 ± 0.05	25.1 ± 0.2	14.8 ± 0.2
	12	11.57 ± 0.02	25.0 ± 0.1	14.6 ± 0.2
	∞	11.59 ± 0.06	25.1 ± 0.2	14.7 ± 0.2

$$\Delta G_i = -k_B T \ln \frac{n_i}{n_1} \quad (1)$$

where n_i and n_1 are the number densities of clusters of size i and of monomers, respectively. For the lower vapor density, the nucleation free energies for $n \leq 8$ are statistically indistinguishable for all values of r_{cut}, but deviations become significant for $n > 8$ with $r_{cut} = 6$ Å, for $n > 20$ with $r_{cut} = 8$ Å, and for $n > 45$ with $r_{cut} = 10$ Å, whereas the data for $r_{cut} = 12$ and ∞ Å agree up to the the size of the critical nucleus, n^*, the value of n where the (unary) nucleation free energy profile reaches its maximum. Thus, the nucleation free energies overlap through an increasingly large range of cluster sizes as the cutoff is increased. As should be expected from this observation, a shorter cutoff can yield satisfactory results for the computation of the nucleation free energy at a higher vapor density (see Fig. 2) because of the decrease in the critical cluster size.

The numerical data for the nucleation free energy barrier, ΔG^*, and the size of the critical nucleus are listed in Table 5. These data were obtained by locating the maximum in a sixth-order polynomial fit to the nucleation free energy profile for each independent simulation. As can be seen, a NGB truncation with $r_{cut} = 10$ Å yields satisfactory results for the higher supersaturation with a critical nucleus consisting of about 15 molecules, while a slightly larger value of $r_{cut} = 12$ Å is needed for the lower supersaturation with a critical nucleus consisting of about 75 molecules.

Using the grand canonical ensemble for the computation of the nucleation free energy profiles, the savings in the computational expense due to the use of a NGB truncation is minimal because only the cluster is treated explicitly. In contrast, we expect considerable gains in efficiency for nucleation simulations in the isobaric–isothermal ensemble, where both the cluster and the surrounding vapor phase are treated explicitly. For simulations employing an electronic structure method, such as the EE-MB approach, to compute the energy, the isobaric–isothermal ensemble formalism is more convenient for the determination of nucleation free energy profiles [22, 24].

3.4 Vapor–liquid phase equilibria for water and hydrogen fluoride

Table 6 lists the vapor and liquid densities, saturated vapor pressures, and heats of vaporization for TIP4P water and OPLS hydrogen fluoride at three temperatures obtained from *NVT*-Gibbs ensemble simulations for which the ES technique is used either for both phases or only for the

Table 6 Coexistence properties for water and hydrogen fluoride: Vapor density (ρ_{gas}), liquid density (ρ_{liq}), vapor pressure (P_{sat}), and heat of vaporization (ΔH_{vap}) calculated from *NVT*-Gibbs ensemble simulations for which the ES method is used for both boxes (ES/ES) or only for the liquid box in conjunction with a NGB truncation for the vapor box (ES/NGB)

Compound	Method	T (K)	ρ_{gas} (kg/m^3)	ρ_{liq} (kg/m^3)	P_{sat} (kPa)	ΔH_{vap} (kJ/mol)
H_2O	ES/ES	300	0.039 ± 0.001	991 ± 1	5.31 ± 0.08	43.60 ± 0.03
	ES/NGB	300	0.038 ± 0.001	992 ± 2	5.23 ± 0.09	43.60 ± 0.06
	ES/ES	450	8.1 ± 0.3	829 ± 2	1,380 ± 30	32.3 ± 0.2
	ES/NGB	450	8.2 ± 0.1	830 ± 2	1,390 ± 10	32.2 ± 0.1
	ES/ES	520	40 ± 2	684 ± 4	5,700 ± 200	22.7 ± 0.3
	ES/NGB	520	43 ± 3	680 ± 3	5,900 ± 200	22.3 ± 0.6
HF	ES/ES	260	1.0 ± 0.1	1,064 ± 1	42 ± 2	9.9 ± 0.6
	ES/NGB	260	1.0 ± 0.2	1,063 ± 1	41 ± 4	9.8 ± 0.6
	ES/ES	300	4.2 ± 0.5	955 ± 3	220 ± 10	11.6 ± 0.8
	ES/NGB	300	4.5 ± 0.6	957 ± 2	220 ± 20	11.2 ± 0.8
	ES/ES	360	27 ± 3	753 ± 4	1,420 ± 50	10.3 ± 0.5
	ES/NGB	360	27 ± 2	749 ± 6	1,460 ± 30	10.1 ± 0.3

liquid phase in conjunction with the NGB truncation for the vapor phase. Phase coexistence properties are extremely sensitive to minor changes in potential truncation or treatment of the long-range interactions when applied to both phases. In the saturated vapor phase, aggregation is usually more prevalent at high reduced temperatures ($T^* = T/T_{crit}$, where T_{crit} is the critical temperature) because of the exponential increase in the vapor density. However, the simulation data for water and hydrogen fluoride covering a range from low to high reduced temperatures do not reveal any statistically significant differences between the two methods of treating the electrostatic interactions in the vapor phase (in comparison, such differences would be large in the liquid phase). Thus, the less expensive NGB cutoff can be used to treat dipole–dipole interactions in the vapor phase without losing accuracy in GEMC simulations. However, it should be noted that most of the computer time in GEMC simulations is spent computing the interactions in the liquid phase and, hence, we observe only a decrease of about 10% in CPU time when replacing the ES technique for the vapor phase with the NGB truncation (this holds only when an appropriate r_{cut} value close to 0.4 L_{box} is used for the ES technique; a smaller value of, say, $r_{cut} = 14$ Å can lead to very substantial increases in CPU time at low reduced temperatures where the volume of the vapor box needs to be large to contain a sufficient number of molecules). Given that only a small fraction of the computer time is spent for the energy calculations in the vapor phase, different truncation distances for the NGB cutoff were not explored for the GEMC simulations.

4 Conclusions

There have been many efforts to address the proper and practical handling of electrostatic interactions, which is one of the most computationally demanding tasks in molecular simulations. The Ewald summation method is one of the most widely used approaches for simulations of condensed phases. However, it has not previously been investigated whether this relatively expensive method is necessary for simulations of vapor phases containing neutral, but dipolar and hydrogen-bonding, molecules and their clusters.

In this study, we have simulated isolated clusters, the superheated vapor phase of hydrogen fluoride, the nucleation free energy for the supersaturated vapor phase of water, and the vapor–liquid equilibria of water and hydrogen fluoride. For all these systems, we find that, at ambient temperature, the Boltzmann-averaged dipole–dipole interaction energy decays as r^{-6} for $r > 6$ Å and that the averaged dipole–dipole interaction energy becomes less than the thermal energy for $r > 12$ Å. Simulations of the bulk vapor phases at various state points demonstrate that a neutral-group-based truncation can produce satisfactory results, and Ewald summation is not necessary for the vapor phases. The suitable value of the neutral-group-based cutoff depends on the spatial size of the vapor-phase aggregates, i.e., the interaction of molecules in the vapor region surrounding an aggregate has no significant effect on the properties and stability of the aggregates. A value of $r_{cut} = 6$ Å was found sufficient for the superheated vapor phase of hydrogen fluoride where aggregates with 6 or fewer molecules are most prevalent, but a larger value is needed to compute the vapor-to-liquid nucleation free energy barrier at modest supersaturation where the critical nucleus contains tens of molecules. Use of spherical truncations results in a considerable saving of computer time for these vapor phases.

Furthermore, the present study indicates that spherical truncation approaches can be applied to the surrounding molecules that generate the field used in the electrostatically embedded many-body methods [26–28]. In addition, the number of dimer or trimer calculations can likely be reduced by using spherical truncation methods. Finally, it should be stressed that the use of the spherical truncation is only appropriate for thermally averaged systems because the truncation error for specific orientations is significantly larger.

Acknowledgments The authors are grateful to Neeraj Rai and Hannah Leverentz for helpful discussions. This work was supported in part by grants CBET-0756641, CHE-0956776, CHE-1051396, and CHE09-56776 from the National Science Foundation and by a seed grant and computer resources from the Minnesota Supercomputing Institute.

References

1. Allen MP, Tildesley DJ (1987) Computer simulation of liquids. Oxford University Press, Oxford
2. Frenkel D, Smit B (2002) Understanding molecular simulation: from algorithms to applications. Academic Press, San Diego
3. Perram JW, Petersen HG, DeLeeuw SW (1988) Mol Phys 65:875
4. Sagui C, Darden TA (1999) Annu Rev Biophys Biomol Struc 28:155
5. Aguado A, Madden PA (2003) J Chem Phys 119:7471
6. Darden T, York D, Pedersen L (1993) J Chem Phys 98:10089
7. Essmann U, Perera L, Berkowitz ML, Darden T, Lee H, Pedersen LG (1995) J Chem Phys 105:8573
8. York DM, Darden TA, Pedersen LG (1993) J Chem Phys 99:8345
9. Feller SE, Pastor RW, Rojnuckarin A, Bogusz S, Brooks BR (1996) J Phys Chem 100:17011
10. Moreno-Razo JA, Diaz-Herrera E, Klapp SHL (2006) Mol Phys 104:2841
11. Fennell CJ, Gezelter JD (2006) J Chem Phys 124:234104
12. Kolafa J, Moucka F, Nezbeda I (2008) Coll Czech Chem Comm 73:481
13. Reif MM, Krautler V, Kastenholz MA, Daura X, Hunenberger PH (2009) J Phys Chem B 113:3112

14. Takahashi K, Narumi T, Yasuoka K (2010) J Chem Phys 133:014109
15. Tsangaris DM, De Pablo JJ (1994) J Chem Phys 101:1477
16. Visco DP, Kofke DA (1998) J Chem Phys 109:4015
17. Ten Wolde PR, Oxtoby DW, Frenkel D (1999) J Chem Phys 111:4762
18. Kathmann SM, Schenter GK, Garrett BC, Chen B, Siepmann JI (2009) J Phys Chem C 113:10354
19. Panagiotopoulos AZ (1987) Mol Phys 61:813
20. Panagiotopoulos AZ, Quirke N, Stapleton M, Tildesley DJ (1988) Mol Phys 63:527
21. De Pablo JJ, Prausnitz JM, Strauch HJ, Cummings PT (1990) J Chem Phys 93:7355
22. McGrath MJ, Siepmann JI, Kuo IFW, Mundy CJ, Vande Vondele J, Hutter J, Mohamed F, Krack M (2006) J Phys Chem A 110:640
23. Anderson KE, Siepmann JI, McMurry PH, Vande Vondele J (2008) J Amer Chem Soc 130:14144
24. McGrath MJ, Ghogomu JN, Mundy CJ, Kuo IFW, Siepmann JI (2010) Phys Chem Chem Phys 12:7678
25. Brooks BR, Bruccoleri RE, Olafson BD, States DJ, Swaminathan S, Karplus M (1983) J. Comp Chem 4:187
26. Dahlke E, Truhlar D (2007) J Theor Comput Chem 3:46
27. Dahlke E, Leverentz H, Truhlar D (2008) J Theor Comput Chem 4:33
28. Leverentz H, Truhlar D (2009) J Theor Comput Chem 5:1573
29. Speetzen ED, Leverentz HR, Lin H, Truhlar DG (2010). In: Manby F (eds) Accurate condensed-phase electronic structure theory. Taylor and Francis, New York, p 105
30. Monte Carlo for Complex Chemical Systems—Minnesota, version 10.1, http://www.chem.umn.edu/groups/siepmann/software.html
31. Cournoyer ME, Jorgensen WL (1984) Mol Phys 51:119
32. Jorgensen WL, Chandrasekhar J, Madura JD, Impey RW, Klein ML (1983) J Chem Phys 79:926
33. Metropolis N, Rosenbluth AW, Rosenbluth MN, Teller A, Teller E (1953) J Chem Phys 21:1087
34. McDonald IR (1972) Mol Phys 23:41
35. Simons J, Hildebrand JH (1924) J Am Chem Soc 46:2183
36. Chen B, Siepmann JI (2000) J Phys Chem B 104:8725
37. Chen B, Siepmann JI (2001) J Phys Chem B 105:11,275
38. Siepmann JI, Frenkel D (1992) Mol Phys 75:59
39. Esselink K, Loyens LDJC, Smit B (1995) Phys Rev E 51:1560
40. Chen B, Potoff JJ, Siepmann JI (2001) J Phys Chem B 105:3093
41. Chen B, Siepmann JI, Klein ML (2005) J Phys Chem A 109:1137
42. Stillinger FH (1963) J Chem Phys 38:1486
43. Chen B, Siepmann JI, Oh KJ, Klein ML (2002) J Chem Phys 116:4317
44. Mooij GCAM, Frenkel D, Smit B (1992) J Phys Cond Mat 4:L255
45. Laso M, de Pablo JJ, Suter UW (1992) J Chem Phys 97:2817
46. Maitland G, Rigby M, Smith EB, Wakeham WA (1981) Intermolecular forces: their origin and determination. Clarendon Press, Oxford
47. Reed AE, Curtiss LA, Weinhold F (1988) Chem Rev 88:899
48. Maerzke KA, Siepmann JI (2010) J Phys Chem B 114:4261
49. Suhm MA (1995) Ber Bunsen-Ges 99:1159
50. Truhlar DG (1990) In: Halbenstadt N, Janda KC (eds) Dynamics of polyatomic van der Waals complexes. Plenum, New York, p 159
51. Galindo A, Burton SJ, Jackson G, Visco DP, Kofke DA (2002) Mol Phys 100:2241
52. Chen B, Siepmann JI (2006) J Phys Chem B 110:3555
53. Curtiss LA, Blander M (1988) Chem Rev 88:827
54. Vlugt TJH, Martin MG, Smit B, Siepmann JI, Krishna R (1998) Mol Phys 94:727
55. Oh KJ, Zeng XC (2000) J Chem Phys 112:294
56. Oh KJ, Zeng XC, Reiss H (1997) J Chem Phys 107:1242